

# LIGHT-FRONT ANALYSIS OF $\pi^-$ MESONS PRODUCED IN Mg - Mg COLLISIONS AT 4.3 A GeV/c.

**M. Anikina<sup>1</sup>, L.Chkhaidze<sup>2</sup>, T.Djobava<sup>2</sup>, V.Garsevanishvili<sup>3,4</sup>,  
L.Kharkhelaury<sup>2</sup>**

<sup>1</sup> Joint Institute for Nuclear Research, 141980 Dubna, Russia

<sup>2</sup> High Energy Physics Institute, Tbilisi State University,  
University Str. 9, 380086 Tbilisi, Republic of Georgia

<sup>3</sup> Mathematical Institute of the Georgian Academy of Sciences  
M.Alexidze Str. 1 , 380093 Tbilisi, Republic of Georgia

<sup>4</sup> CERN, CH-1211, Geneva 23, Switzerland

E-mail: djobava@sun20.hepi.edu.ge

## ABSTRACT

Light-front analysis of  $\pi^-$  mesons in Mg-Mg collisions is carried out. The phase space of secondary pions is naturally divided into two parts in one of which the thermal equilibration assumption seems to be in a good agreement with data. Corresponding temperatures are extracted and compared to the results of other experiments. The experimental results have been compared with the predictions of the Quark Gluon String Model (QGSM) and satisfactory agreement between the experimental data and the model has been found.

**PACS.** 25.70.-z

**Keywords:** **NUCLEAR REACTION** Mg(Mg,  $\pi^-$  X), at P=4.3 A GeV/c;  
measured pion distributions; the analysis in light front variables  
is carried out; deduced thermal equilibration, which is characterized  
by the temperature T; Comparison with Quark Gluon String Model.

## 1. INTRODUCTION

In the experiments with beams of relativistic heavy ions one hopes to observe the extreme conditions when the phase transitions in nuclear matter are expected (see, e.g. [1-3]).

For the experimental study of such transitions it is necessary to understand the mechanism of collisions and investigate the characteristics of multiparticle production in nucleus-nucleus interactions. The study of single particle inclusive processes is one of the simplest and effective tools for the understanding of dynamics of multiple production of secondaries.

In this respect it is important to investigate the properties of  $\pi^-$  mesons, which are predominantly produced particles carrying the information about the dynamics of collision and which are reliably identified. Besides, the pion production is the predominant process at Dubna energies.

Our previous results on pion production experiment (cross-sections, multiplicities, rapidities, transverse momenta, intercorrelations between various characteristics, etc) using the streamer chamber spectrometer SKM-200 and its modified version GIBS in inelastic and central nucleus-nucleus interactions are presented in [4-6].

In this paper we present the light front analysis of  $\pi^-$  mesons produced in Mg-Mg collisions. It is assumed that interactions of identical nuclei (Mg-Mg) give the possibility of better manifestation of nuclear effects than the interactions of asymmetric pairs. In some cases light front analysis [7] seems to be more sensitive to the details of the interaction mechanism as compared to the presentation of data in terms of the well known Feynman variables  $x_F$ , rapidity  $Y$  etc.

## 2. EXPERIMENT

The data were obtained using the SKM-200 facility and its modified version GIBS of the Dubna Joint Institute for Nuclear Research. SKM-200-GIBS consists of a 2m streamer chamber, placed in a magnetic field of  $\sim 0.8$  T and a triggering system. The streamer chamber was exposed by beam of Mg nuclei accelerated in the synchrophasotron up to a momentum of 4.3 GeV/c per incident nucleon. The solid target (Mg) in the form of thin disc with thickness 1.56 g/cm<sup>2</sup> was mounted within the fiducial volume of the chamber. The triggering system allowed the selection of "inelastic" and "central" collisions.

The inelastic trigger selected all inelastic interactions of the incident nuclei on the target. The central trigger selected events defined as those without charged and neutral projectile spectator fragments ( $P/Z > 3 \text{ GeV}/c$ ) within a cone of half angle  $\Theta_{ch}=\Theta_n=2.4^\circ$  (the trigger efficiency was 99% for events with a single charged particle and 80% for events with a single neutron in the cone). The trigger mode for each exposure is defined as  $T(\Theta_{ch}, \Theta_n)$  ( $\Theta_{ch}$  and  $\Theta_n$  expressed in degrees and rounded to the closest integer value). Thus Mg-Mg interactions obtained on the set-up correspond to the trigger  $T(2,2)$ . The fraction of such events was  $\approx 4 \cdot 10^{-4}$  among all inelastic interactions. The experimental setup and the logic of the triggering systems are presented in Fig.1.

Primary results of scanning and measurements were biased due to several experimental effects and appropriate corrections were introduced. The biases and correction procedures were discussed in detail in [4,6]. Average measurement errors of the momentum and production angle determination for  $\pi^-$  mesons are  $< \Delta P/P > = 1.5\%$ ,  $\Delta\Theta = 0.1^\circ$ .

### 3. LIGHT FRONT PRESENTATION OF INCLUSIVE DISTRIBUTIONS

An important role in establishing of many properties of multiple production is played by the choice of kinematical variables in terms of which observable quantities are presented (see in this connection, e.g. [8]).

Here we propose unified scale invariant variables for the presentation of single particle inclusive distributions, the properties of which are described below.

Consider an arbitrary 4-momentum  $p_\mu(p_0, \vec{p})$  and introduce the light front combinations [9]:

$$p_\pm = p_0 \pm p_3 \quad (1)$$

If the 4-momentum  $p_\mu$  is on the mass shell ( $p^2 = m^2$ ), the combinations  $p_\pm$ ,  $\vec{p}_T$  (where  $\vec{p}_T = (p_1, p_2)$ ) define the so called horospherical coordinate system (see, e.g. [10]) on the corresponding mass shell hyperboloid  $p_0^2 - \vec{p}^2 = m^2$ .

Let us construct the scale invariant variables [7]:

$$\xi^\pm = \pm \frac{p_\pm^c}{p_\pm^a + p_\pm^b} \quad (2)$$

in terms of the 4-momenta  $p_\mu^a$ ,  $p_\mu^b$ ,  $p_\mu^c$  of particles  $a$ ,  $b$ ,  $c$ , entering the inclusive reaction  $a + b \rightarrow c + X$ . The  $z$ -axis is taken to be the collision axis, i.e.  $p_z = p_3 = p_L$ . Particles

$a$  and  $b$  can be hadrons, heavy ions, leptons. The light front variables  $\xi^\pm$  in the centre of mass frame are defined as follows [7]:

$$\xi^\pm = \pm \frac{E \pm p_z}{\sqrt{s}} = \pm \frac{E + |p_z|}{\sqrt{s}} \quad (3)$$

where  $s$  is the usual Mandelstam variable,  $E = \sqrt{p_z^2 + p_T^2 + m^2}$  and  $p_z$  are the energy and the  $z$  - component of the momentum of produced particle. The upper sign in Eq. (3) is used for the right hand side hemisphere and the lower sign for the left hand side hemisphere. It is convenient also to introduce the variables

$$\zeta^\pm = \mp \ln |\xi^\pm|$$

in order to enlarge the scale in the region of small  $\xi^\pm$ .

The invariant differential cross section in terms of these variables looks as follows:

$$E \frac{d\sigma}{d\vec{p}} = \frac{|\xi^\pm|}{\pi} \frac{d\sigma}{d\xi^\pm dp_T^2} = \frac{1}{\pi} \frac{d\sigma}{d\zeta^\pm dp_T^2} \quad (4)$$

In the limits of high  $p_z$  ( $|p_z| \gg p_T$ ) and high  $p_T$  ( $p_T \gg |p_z|$ ) the  $\xi^\pm$  variables go over to the well known variables  $x_F = 2p_z/\sqrt{s}$  and  $x_T = 2p_T/\sqrt{s}$ , respectively, which are intensively used in high energy physics.  $\xi^\pm$ -variables are related to  $x_F$ ,  $x_T$  and rapidity  $y$  as follows:

$$\xi^\pm = \frac{1}{2} \left( x_F \pm \sqrt{x_F^2 + x_T^2} \right) ; \quad x_T = \frac{2m_T}{\sqrt{s}} \quad (5)$$

$$y = \pm \frac{1}{2} \ln \frac{(\xi^\pm \sqrt{s})^2}{m_T^2} ; \quad m_T = \sqrt{p_T^2 + m^2} \quad (6)$$

The principal differences of  $\xi^\pm$  distributions as compared to the corresponding  $x_F$  - distributions are the following: 1) existence of some forbidden region around the point  $\xi^\pm = 0$ , 2) existence of maxima at some  $\xi^\pm$  in the region of relatively small  $|\xi^\pm|$ , 3) existence of the limits for  $|\xi^\pm| \leq m/\sqrt{s}$ . The maximum at  $\tilde{\zeta}^\pm$  is also observed in the invariant differential cross section  $\frac{1}{\pi} \frac{d\sigma}{d\zeta^\pm}$ . However, the region  $|\xi^\pm| > |\tilde{\xi}^\pm|$  goes over to the region  $|\zeta^\pm| < |\tilde{\zeta}^\pm|$  and vice versa.

Note that the light front variables have been introduced long time ago by Dirac [9] and they are widely used now in the treatment of many theoretical problems (see, e.g. original and review papers [11-19] and references therein). They have been used also in a number of phenomenological applications (see, e.g. [20]).

#### 4. THE ANALYSIS OF PION DISTRIBUTIONS IN TERMS OF LIGHT FRONT VARIABLES.

The analysis has been carried out for the  $\pi^-$  mesons from central (trigger T(2,2)) Mg-Mg collisions ( $\sim 6200$  events,  $\sim 50\,000$   $\pi^-$  mesons). In Figs.2 and 3  $x_F$  – and  $\xi^\pm$  – distributions of all  $\pi^-$  mesons are presented. The experimental data for invariant distribution  $(1/\pi) \cdot dN/d\zeta^\pm$  are shown in Fig.4. The curve is the result of the polinomial approximation of the experimental distribution and the maximum is observed at  $\tilde{\zeta}^\pm = 2.0 \pm 0.3$ . The value  $\tilde{\zeta}^\pm$  is the boundary of the two regions with significantly different characteristics of secondaries.

In Figs.5 and 6 the  $p_T^2$  and the angular distributions of  $\pi^-$  mesons in the forward hemisphere in different regions of  $\zeta^+$  ( $\zeta^+ > \tilde{\zeta}^+$  and  $\zeta^+ < \tilde{\zeta}^+$ ) are presented. Similar results have been obtained for the backward emitting  $\pi^-$  mesons.

One can see from Figs.5 and 6, that the  $p_T^2$  and angular distributions of  $\pi^-$  mesons differ significantly in  $\zeta^+ > \tilde{\zeta}^+$  ( $\xi^+ < \tilde{\xi}^+$ ) and  $\zeta^+ < \tilde{\zeta}^+$  ( $\xi^+ > \tilde{\xi}^+$ ) regions. The angular distribution of pions in the region  $\zeta^+ < \tilde{\zeta}^+$  is sharply anisotropic in contrast to the almost flat distribution in the region  $\zeta^+ > \tilde{\zeta}^+$ . The slopes of  $p_T^2$  – distributions differ greatly in different regions of  $\zeta^+$ . The average values  $\langle p_T^2 \rangle$  in these two regions also differ:  $\langle p_T^2 \rangle = (0.027 \pm 0.002)$  (GeV/c) $^2$  in the region  $\zeta^+ > \tilde{\zeta}^+$ ;  $\langle p_T^2 \rangle = (0.103 \pm 0.009)$  (GeV/c) $^2$  in  $\zeta^+ < \tilde{\zeta}^+$ .

The flat behaviour of the angular distribution allows one to think that one observes a partial thermal equilibration in the region  $|\xi^\pm| < |\tilde{\xi}^\pm|$  ( $|\zeta^\pm| > |\tilde{\zeta}^\pm|$ ) of phase space.

Note, that the paraboloids of constant  $\xi^+$

$$p_z = \frac{p_T^2 + m^2 - (\tilde{\xi}^+ \sqrt{s})^2}{-2\tilde{\xi}^+ \sqrt{s}} \quad (7)$$

separates two groups of particles with significantly different characteristics.

To describe the spectra in the region  $\zeta^+ > \tilde{\zeta}^+$  the Boltzmann  $f(E) \sim e^{-E/T}$  and the Bose-Einstein (B-E)  $f(E) \sim (e^{-E/T} - 1)^{-1}$  distributions have been used.

The distributions  $(1/\pi) \cdot dN/d\zeta^+$ ,  $dN/dp_T^2$ ,  $dN/d\cos\Theta$  look in this region as follows :

$$\frac{d\sigma}{dp_T^2} \sim \int_0^{p_{z,max}} f(E) dp_z \quad (8)$$

$$\frac{d\sigma}{d\cos\theta} \sim \int_0^{p_{max}} f(E) p^2 dp \quad (9)$$

$$\frac{1}{\pi} \frac{d\sigma}{d\zeta^+} \sim \int_0^{p_{T,max}^2} E f(E) dp_T^2 \quad (10)$$

where:

$$\begin{aligned}
p_{T,max}^2 &= (\tilde{\xi}^+ \sqrt{s})^2 - m_\pi^2 \\
p_{z,max} &= [p_T^2 + m^2 - (\tilde{\xi}^+ \sqrt{s})^2] / (-2\tilde{\xi}^+ \sqrt{s}) \\
p_{max} &= (-\tilde{\xi}^+ \sqrt{s} \cos \Theta + \sqrt{(\tilde{\xi}^+ \sqrt{s})^2 - m_\pi^2 \sin^2 \Theta}) / \sin^2 \Theta
\end{aligned}$$

The experimental distributions in the region  $\zeta^+ > \tilde{\zeta}^+$  have been fitted by the expressions (8), (9), (10), respectively. The results of the fit are given in Table 1 and Figs. 5 ÷ 7 (by the Boltzmann distribution). They show a rather good agreement with experiment. One can see from the Table 1, that the values of the parameter  $T$  extracted by fitting the data with Boltzmann and Bose-Einstein distributions coincide within the errors.

In the region  $\zeta^+ < \tilde{\zeta}^+$  the  $p_T^2$  - distributions has been fitted by the formula

$$\frac{dN}{dp_T^2} \sim \alpha \cdot e^{-\beta_1 p_T^2} + (1 - \alpha) \cdot e^{-\beta_2 p_T^2} \quad (11)$$

and the  $\zeta^+$  - distributions by the formula

$$\frac{1}{\pi} \cdot \frac{dN}{d\zeta^+} \sim (1 - \xi^+)^n = (1 - e^{-|\zeta^+|})^n \quad (12)$$

The results of the fit are given in Table 2 and Figs. 5 and 7.

Thus the spectra of  $\pi^-$  mesons in the region  $\zeta^+ > \tilde{\zeta}^+$  are satisfactorily described by the formulae which follow from the thermal equilibration. The same formulae when extrapolated to the region  $\zeta^+ < \tilde{\zeta}^+$  (Fig. 7) deviate significantly from the data. On the other hand the dependence  $(1 - \xi^+)^n$  is in a good agreement with experiment in the region  $\zeta^+ < \tilde{\zeta}^+$  and deviates from it in the region  $\zeta^+ > \tilde{\zeta}^+$  (Fig. 7).

Several theoretical models of nucleus-nucleus collisions at high energy have been proposed [21]. In this paper Quark Gluon String Model (QGSM) [22] is used for a comparison with experimental data. The QGSM is based on the Regge and string phenomenology of particle production in inelastic binary hadron collisions [23]. The QGSM simplifies the nuclear effects (neglects the potential interactions between hadrons, coalescence of nucleons and etc.). A detailed description and comparison of the QGSM with experimental data in a wide energy range can be found in paper [24]. To describe the evolution of the hadron and quark-gluon phases, this model uses a coupled system of Boltzmann-like kinetic equations. Nuclear collisions are treated as a mixture of independent interactions of the projectile and target nucleons, stable hadrons and short lived resonances. QGSM includes low mass vector mesons and baryons with spin 3/2, mostly  $\Delta(3/2, 3/2)$  resonances. The procedure of generation consists of 3 steps: the definition of configuration of

colliding nuclei, production of quark-gluon strings and fragmentation of strings (breakup) into observed hadrons. The formation time of hadrons is also included in the model. The QGSM has been extrapolated to the range of intermediate energy ( $\sqrt{s} \leq 4$  GeV) to use it as a basic process during the generation of hadron-hadron collisions. After hadronization the newly formed secondary hadrons are allowed to rescatter. To determine the interaction between hadrons, the experimental total, elastic, and annihilation cross sections have been used. Isotopic invariance and the additive quark model relations were used to avoid data deficiency. The resonance cross sections were assumed to be identical to the stable particle cross sections with the same quark content. At low energy the QGSM reduces to a standard cascade model without mean field effects. The model yields a generally good overall fit to most experimental data [24,25]. Particularly the model describes well the average kinematical characteristics and distributions of pions in Mg-Mg interactions [26].

We have generated Mg-Mg interactions using Monte-Carlo generator COLLI, based on the QGSM. The events had been traced through the detector and trigger filter.

In the generator COLLI there are two possibilities to generate events: 1) at not fixed impact parameter  $\tilde{b}$  and 2) at fixed  $b$ . The events have been generated for  $\tilde{b}$  ( $0 \leq \tilde{b} \leq 6$  fm). The number of simulated events is  $\sim 4000$ . From the impact parameter distribution we obtained the mean value of  $\langle b \rangle = 1.34 \pm 0.02$  fm. For the obtained value of  $\langle b \rangle$ , we have generated a total sample of 6200 events. The two regimes are consistent and it seems, that in our experiment the value of  $b=1.34$  fm for Mg-Mg is most probable.

The experimental results have been compared with the predictions of the QGSM for  $b=1.34$  fm and satisfactory agreement between the experimental data and the model have been found. In Figs 2, 3 and 4 the  $x_F$ ,  $\xi^\pm$  and  $\zeta^\pm$  - distributions of  $\pi^-$  mesons from the QGSM calculations are presented together with the experimental ones. One can see, that the QGSM reproduces these distributions. The QGSM also reproduces the  $p_T^2$  and  $\cos\Theta$  distributions (Figs.5 and 6). The QGSM data show the similar characteristics in the different regions of  $\zeta$  as experimental ones: sharply anisotropic angular distributions in the region  $\zeta^+ < \tilde{\zeta}^+$  and the almost flat distribution in the region  $\zeta^+ > \tilde{\zeta}^+$ . The slopes of  $p_T^2$  - distributions differ greatly in different regions of  $\zeta^+$ . The average values  $\langle p_T^2 \rangle$  in these two regions also differ:  $\langle p_T^2 \rangle = (0.029 \pm 0.003) \text{ (GeV/c)}^2$  in the region  $\zeta^+ > \tilde{\zeta}^+$ ;  $\langle p_T^2 \rangle = (0.109 \pm 0.009) \text{ (GeV/c)}^2$  in  $\zeta^+ < \tilde{\zeta}^+$ . The average values of  $\langle p_T^2 \rangle$  in the different regions of  $\zeta$  from the experimental and QGSM data are in a good agreement between each other. The distributions obtained by the QGSM in the region  $\zeta^+ > \tilde{\zeta}^+$  have been fitted by the expressions (8), (9), (10). The results of the fit are given in Table 1 and Figs. 5  $\div$  7. In the region  $\zeta^+ < \tilde{\zeta}^+$  the  $p_T^2$  and the  $\zeta^+$  - distributions have been fitted by the formulae (11) and (12), respectively. The results of the fit are given in Table

2 and Figs.5 and 7 (by the Boltzmann distribution). One can see from the Table 1, that the values of the  $T$  extracted from the experimental and QGSM data coincide within the errors, only for the  $(1/\pi) \cdot dN/d\zeta^+$  distribution the QGSM slightly overestimates the experimental result (for the B-E distribution).

In our previous article [27] the  $\pi^-$  mesons temperature in Mg-Mg collisions was estimated by means of inclusive kinetic energy and transverse momentum spectra for  $\pi^-$  mesons: in rapidity interval  $0.5 \div 2.1$ , which corresponds to the pionization region for  $\pi^-$  mesons and with the c.m.s. angles  $90^\circ \pm 10^\circ$ . The pion spectra have been fitted by a sum of two exponentials, or two temperatures  $T_1$  and  $T_2$ .  $T_1 = 55 \pm 1$  MeV,  $T_2 = 113 \pm 2$  MeV. This explained by two mechanisms of pion production: directly ( $T_2$ ) and via  $\Delta$  resonance decay ( $T_1$ ). The relative yield of  $T_2$  is  $\approx 22\%$ . One can see, that the light front analysis gives temperature which is weighted average value of  $T_1$  and  $T_2$ . The temperatures of pions have been extracted in the GSI experiments (FOPI, FRS, KAON and TAPS- Collaborations, see, e.g. [28,29]) similarly. At FOPI Collaboration [28] it has been obtained that the  $\pi^-$  spectra from Ni-Ni collisions require the sum of two exponential functions with independent yields and slope parameters  $T_l$  and  $T_h$  describing mostly the low and the high momentum part of the spectrum, respectively: at  $E=1.06$  A GeV  $T_l = 55 \pm 3$  MeV,  $T_h = 93 \pm 5$  MeV; at  $E=1.45$  A GeV  $T_l = 56 \pm 3$  MeV,  $T_h = 100 \pm 5$  MeV; at  $E=1.93$  A GeV  $T_l = 61 \pm 3$  MeV,  $T_h = 115 \pm 6$  MeV. At FRS Collaboration it has been obtained that the  $T$  for  $\pi^-$  mesons in Ne-NaF collisions range from  $78 \pm 2$  MeV to  $96 \pm 3$  MeV for projectile energies from 1.34 to 1.94 A GeV. At TAPS Collaboration for  $\pi^0$  mesons:  $T = 83 \pm 3$  MeV in C-C interactions at incident energy of  $E=2$  A GeV;  $T = 70 \pm 1$  MeV in Ar-Ca interactions at incident energy of  $E=1.5$  A GeV; At KAON Collaboration the value of  $T$  for  $\pi^+$  mesons ranges from  $71 \pm 3$  MeV (at energy  $E=1$  A GeV) to  $95 \pm 3$  MeV (at energy  $E=1.8$  A GeV).

It should be noted that the extraction procedures of  $T$  in the light front variables and in the GSI experiments are different. It seems to be interesting in this connection to perform the light front analysis of the GSI data.

## 5. CONCLUSIONS

The analysis of  $\pi^-$  – mesons from Mg-Mg collisions in the light front variables has been carried out. In some region of phase space of  $\pi^-$  mesons the thermal equilibration seems to be reached, which is characterized by the temperature  $T = 75 \pm 3$  MeV. The variables



used can serve as a possible convenient tool to study hadron-production processes in hadron-hadron, nucleus-nucleus and  $e^+ e^-$  – interactions.

A remark on the nature of maxima in  $\zeta^\pm$  -distributions is in order. Recently ALEPH Collaboration observed the maxima in the  $\xi$  - distributions ( $\xi = -\ln p/p_{max}$ ) [30] of secondary hadrons in  $e^+ e^-$  collisions, which coincide to high precision with the predictions of perturbative QCD (see., e.g. [31,32]). The accuracy of coincidence increases when the next to leading order corrections are taken into account. So the shapes of  $\xi$  - distributions are related to the details of the underlying dynamics. Similarly, it seems that the maxima in  $\zeta^\pm$  -distributions reflect the dynamics of the processes considered.

The authors express their deep gratitude to J.-P.Alard, N.Amaglobeli, D.Ferenc, Sh.Esakia, S.Khorozov, G.Kuratahashvili, J.Lukstins, J.-F.Mathiot, Z.Menteshashvili, G.Paic, G.Roche for interesting discussions. We are very grateful to N.Amelin for providing us with the QGSM code program COLLI. One of the authors (V.G.) would like to thank A.De Rujula and G.Veneziano and CERN Theory Division for the warm hospitality.

## References

- [1] M.Jacob and J.Tran Thanh Van Phys.Rep. C88(1982)321
- [2] L.Csernai and J.Kapusta Phys.Rep. 131(1986)223
- [3] H.Stöcker and W.Greiner Phys.Rep. 137(1986)277
- [4] M.Anikina et al., JINR Report E1-84-785,Dubna (1984) 17
- [5] M.Anikina et al., Phys.Rev. C33(1986)895
- [6] M.Anikina et al., JINR Rapid Commun. 1[34]-89, Dubna (1989) 12
- [7] N.S.Amaglobeli et al., Report N hep-ph/9703386
- [8] A.M.Baldin, Nucl.Phys. A447(1985)203
- [9] P.A.M.Dirac, Rev.Mod.Phys. 21(1949)392
- [10] N.Ya.Vilenkin and Ya.A.Smorodinsky Sov. J. of Exp. and Theor. Phys. JETP 47(1964)1793;  
V.Garsevanishvili, V.G. Kadyshevsky, R.M.Mir-Kasimov, N.B.Skachkov Sov. J. of Theor. and Math.Phys. 7(1971)203
- [11] V.Garsevanishvili, A.Kvinikhidze, V.Matveev, A.Tavkhelidze, R.Faustov Sov. J. Theor. and Math.Phys. 23(1975)310
- [12] S.J.Chang, R.G.Root, T.M.Yan Phys.Rev. D7(1973)1133
- [13] H.Leutwyler, Nucl.Phys. B76(1974)413
- [14] A.Harindranath and J.Vary Phys.Rev. D36(1987)1141; D37(1988)1064
- [15] S.J.Brodsky, H.C.Pauli In: Recent Aspects of Quantum Fields. Eds. H.Miller, H.Gausterer (Springer Verlag, Berlin, 1991)
- [16] S.J.Brodsky, G.McCartor, H.C.Pauli, S.S.Pinsky. Particle World 3(1993) 109
- [17] V.Garsevanishvili, Z.R.Menteshashvili. Relativistic Nuclear Physics in the Light Front Formalism (Nova Science Publishers, New York, 1993)
- [18] K.G.Wilson, T.S.Walout, A.Harindranath, W.M.Zhang, R.J.Perry, St.D.Glazek Phys.Rev. D49(1994)6720

- [19] B.Desplanques, V.A.Karmanov, J.F.Mathiot Nucl.Phys. A589(1995)697;  
J.Carbonell, B.Desplanques, V.A.Karmanov, J.F.Mathiot. To appear in Phys. Rep.
- [20] B.S.Aladashvili et al. Dubna-Kosice-Moscow-Strasbourg-Tbilisi-Warsaw Collaboration. Sov.J. Nucl.Phys. 34(1981)591;  
L.S.Azhgirey et al., Phys.Lett. B387(1996)37
- [21] S.Nagamiya and M.Gyulassy, Adv.In Nucl.Phys. 13(1984)201
- [22] N.Amelin et al., Phys.Rev.Lett. 67(1991)1523
- [23] B.Andersson, G Gustafsson and B.Nilsson-Almqvist, Nucl.Phys. B281(1987)289
- [24] N.Amelin and L.Csernai, In Proc. of the Int. Workshop on Correlations and Multi-particle Production (CAMP), Marburg, Germany, 1990 (World Scientific, Singapore, 1990);  
N.Amelin, K.Gudima and V.Toneev, Sov.J. Nucl.Phys. 51(1990)327
- [25] N.Amelin et al., Sov.J. Nucl.Phys. 51(1990)535;  
N.Amelin et al., Sov.J. Nucl.Phys. 52(1990)172
- [26] L.Chkhaidze et al., Eur. Phys.J. A 1(1998)3, 299
- [27] L.Chkhaidze et al., J. Phys.G: Nucl. Part. Phys.22(1996)641
- [28] B.Hong et al., Phys.Rev. C57(1998)244
- [29] A.Gilg et al., GSI Scientific Report 96-1, Darmstadt (1996) 52;  
M.Pfeiffer et al., GSI Scientific Report 93-1, Darmstadt (1993) 58;  
O.Schwalb et al., GSI Scientific Report 93-1, Darmstadt (1993) 62;  
M.Appenheimer et al., GSI Scientific Report 97-1, Darmstadt (1997) 58;  
C.Müntz al., GSI Scientific Report 95-1,Darmstadt (1995) 77
- [30] ALEPH Collaboration. CERN/PPE 96-999, to appear in Phys.Rep.
- [31] C.P.Fong and B.R.Webber Phys.Lett. B229(1989)289
- [32] Yu.L.Dokshitzer, V.A.Khoze, A.H.Mueller and S.I.Troyan. Basics of Perturbative QCD. (Editions Frontieres, Gif-sur-Yvette, 1991)

## FIGURE CAPTIONS

**Fig.1** Experimental set-up. The trigger and the trigger distances are not to scale.

**Fig.2** The  $x_F$  – distribution of  $\pi^-$  mesons.  $\circ$  – experimental data,  $*$  – QGSM data.

**Fig.3** The  $\xi^\pm$  – distribution of  $\pi^-$  mesons.  $\circ$  – experimental data,  $*$  – QGSM data. The curve is a result of polinomial approximation of the experimental data.

**Fig.4** The  $\zeta^\pm$  distribution of  $\pi^-$  mesons.  $\circ$  – experimental data,  $*$  – QGSM data. The curve – result of polinomial approximation of the experimental data.

**Fig.5** The  $p_T^2$  distribution of  $\pi^-$  mesons.  $\circ$  – experimental data for  $\zeta^+ > \tilde{\zeta}^+$  ( $\tilde{\zeta}^+=2.0$ ),  $\diamond$  – the QGSM data for  $\zeta^+ > \tilde{\zeta}^+$ ,  $\triangle$  – experimental data for  $\zeta^+ < \tilde{\zeta}^+$ ,  $\square$  – the QGSM data for  $\zeta^+ < \tilde{\zeta}^+$ . The dashed lines - fit of the experimental data by the Boltzmann distribution ; the solid lines - fit of the QGSM data by the Boltzmann distribution.

**Fig.6** The  $\cos\Theta$  distribution of  $\pi^-$  mesons.  $\circ$  – experimental data for  $\zeta^+ > \tilde{\zeta}^+$  ( $\tilde{\zeta}^+=2.0$ ),  $\diamond$  – the QGSM data for  $\zeta^+ > \tilde{\zeta}^+$ ,  $\triangle$  – experimental data for  $\zeta^+ < \tilde{\zeta}^+$ ,  $\square$  – the QGSM data for  $\zeta^+ < \tilde{\zeta}^+$ . The dashed lines - fit of the experimental data by the Boltzmann distribution; the solid lines - fit of the QGSM data by the Boltzmann distribution.

**Fig.7** The  $(1/\pi) \cdot dN/d\zeta^+$  distribution of  $\pi^-$  mesons.  $\circ$  – experimental data, the solid line – fit of the data in the region  $\zeta^+ > \tilde{\zeta}^+$  by the Boltzman distribution, the dashed line – fit of the data in the region  $\zeta^+ < \tilde{\zeta}^+$  by the formula  $(1 - e^{-|\zeta^+|})^n$ ;  $\triangle$  – the QGSM data.

## TABLE CAPTIONS

**Table 1.** The results of the fit of the distributions of  $\pi^-$  – mesons in the region  $\zeta^+ > \tilde{\zeta}^+$ .

**Table 2.** The results of the fit of the distributions of  $\pi^-$  mesons in the region  $\zeta^+ < \tilde{\zeta}^+$

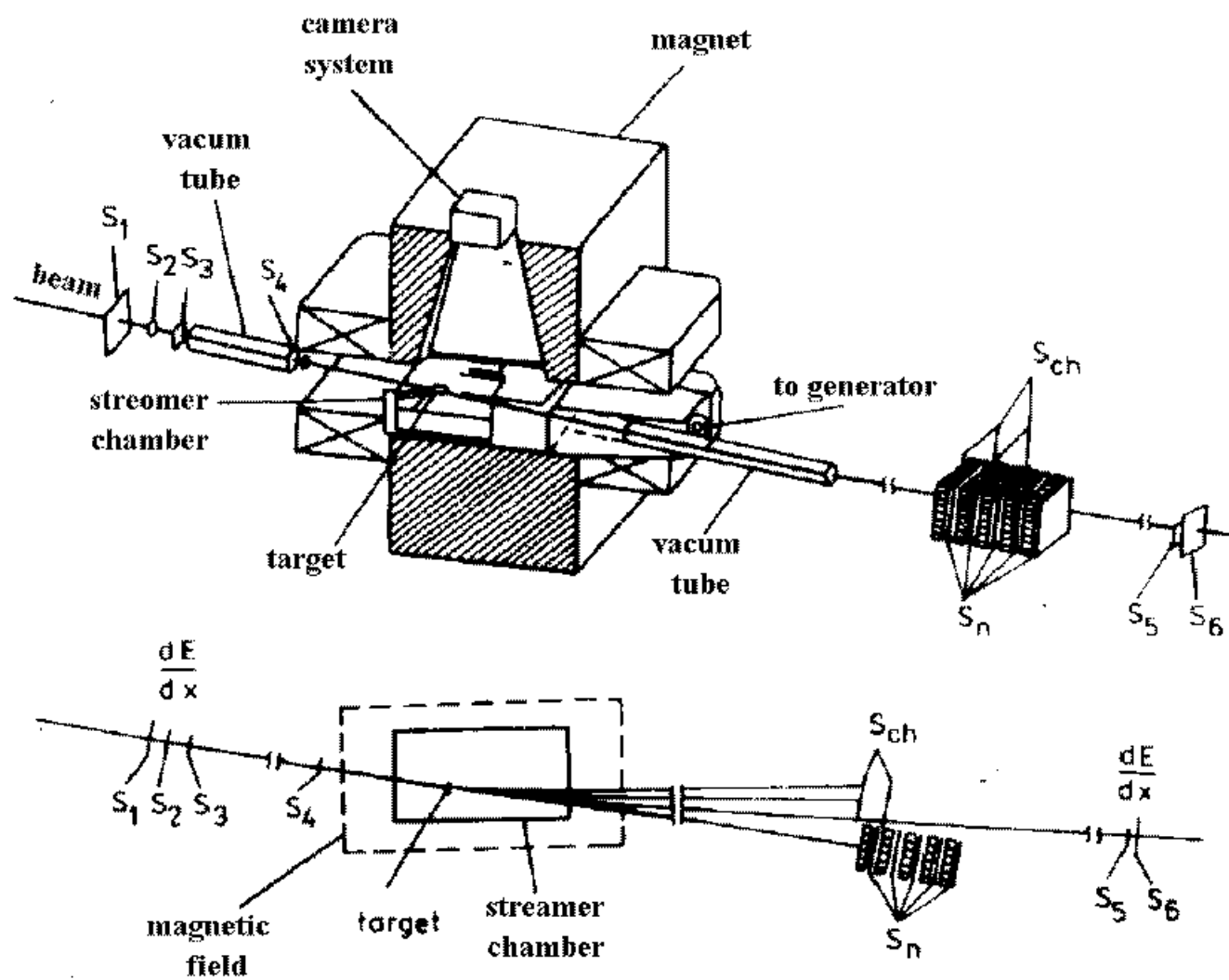
**Table 1.** The results of the fit of the distributions of  $\pi^-$  – mesons in the region  $\zeta^+ > \tilde{\zeta}^+$ .

<i>Type of events</i>	<i>Number of events</i>	<i>T (MeV)</i>					
		$dN/dP_T^2$		$dN/d\cos\Theta$		$1/\pi \cdot dN/d\zeta^+$	
		<i>Boltz</i>	<i>B – E</i>	<i>Boltz</i>	<i>B – E</i>	<i>Boltz</i>	<i>B – E</i>
exp.	6239	$76 \pm 2$	$76 \pm 3$	$75 \pm 3$	$78 \pm 4$	$75 \pm 3$	$75 \pm 4$
QGSM	6212	$77 \pm 2$	$80 \pm 3$	$68 \pm 5$	$69 \pm 5$	$82 \pm 4$	$89 \pm 3$

**Table 2.** The results of the fit of the distributions of  $\pi^-$  mesons in the region  $\zeta^+ < \tilde{\zeta}^+$

	$dN/dp_T^2$			$1/\pi * dN/d\zeta^+$
	$\alpha$	$\beta_1$ $(GeV/c)^{-2}$	$\beta_2$ $(GeV/c)^{-2}$	$n$
exp.	$0.85 \pm 0.03$	$12.0 \pm 0.4$	$4.8 \pm 0.3$	$4.30 \pm 0.06$
QGSM	$0.90 \pm 0.05$	$11.4 \pm 0.6$	$5.2 \pm 0.9$	$4.17 \pm 0.11$

# GIBS



"INELASTIC" TRIGGER =  $S_1 \wedge S_2 \wedge S_3 \wedge S_4 \wedge \bar{S}_5 \wedge \bar{S}_6$

"CENTRAL" TRIGGER =  $S_1 \wedge S_2 \wedge S_3 \wedge S_4 \wedge \bar{S}_n \wedge \bar{S}_{ch}$

